Increasing Antarctic Sea Ice under Warming Atmospheric and Oceanic Conditions

JINLUN ZHANG

Polar Science Center, Applied Physics Laboratory, College of Ocean and Fishery Sciences, University of Washington, Seattle, Washington

(Manuscript received 10 January 2006, in final form 18 September 2006)

ABSTRACT

Estimates of sea ice extent based on satellite observations show an increasing Antarctic sea ice cover from 1979 to 2004 even though in situ observations show a prevailing warming trend in both the atmosphere and the ocean. This riddle is explored here using a global multicategory thickness and enthalpy distribution sea ice model coupled to an ocean model. Forced by the NCEP–NCAR reanalysis data, the model simulates an increase of 0.20×10^{12} m^3 yr^{-1} (1.0% yr^{-1}) in total Antarctic sea ice volume and 0.084×10^{12} m^2 yr^{-1} (0.6% yr^{-1}) in sea ice extent from 1979 to 2004 when the satellite observations show an increase of 0.027×10^{12} m^2 yr^{-1} (0.2% yr^{-1}) in sea ice extent during the same period. The model shows that an increase in surface air temperature and downward longwave radiation results in an increase in the upper-ocean temperature and a decrease in sea ice growth, leading to a decrease in salt rejection from ice, in the upper-ocean salinity, and in the upper-ocean density. The reduced salt rejection and upper-ocean density and the enhanced thermohaline stratification tend to suppress convective overturning, leading to a decrease in the upward ocean heat transport and the ocean heat flux available to melt sea ice. The ice melting from ocean heat flux decreases faster than the ice growth does in the weakly stratified Southern Ocean, leading to an increase in the net ice production and hence an increase in ice mass. This mechanism is the main reason why the Antarctic sea ice has increased in spite of warming conditions both above and below during the period 1979–2004 and the extended period 1948–2004.

1. Introduction

Significant climate changes observed in the Antarctic include the increase in surface air temperature (SAT). SAT over the Antarctic as a whole has increased by 0.5°C in the last 50 yr (Jacka and Budd 1998), which appears to be part of a global SAT warming trend in recent years (e.g., Alley et al. 2003). This increase is reflected in the spatial distribution of the linear SAT trends over 1979–2004 for the ice-covered areas of the Southern Ocean (Fig. 1), based on the National Centers for Environmental Prediction–National Center for Atmospheric Research (NCEP–NCAR) reanalysis data (Kalnay et al. 1996). Except for some areas of the Atlantic and Indian sectors where SAT has decreased, a significant increase in SAT has occurred in most of the Southern Ocean according to the reanalysis data. Since 1979 the increase in SAT is 0.027°C yr^{-1} over the ice-covered areas of the Southern Ocean (Fig. 2a; Table 1). In conjunction with an increase in SAT is an increase in the NCEP–NCAR reanalysis surface downward longwave radiation (SDLR) and precipitation (Figs. 2b,c; Table 1).

Moreover, since the 1950s the Southern Ocean has been warming faster than other oceans in the world (Gille 2002); the average global ocean temperature in the upper 1000 m has increased by 0.1°C between 1955 and 1995 (Levitus et al. 2000), whereas the middepth Southern Ocean temperatures have increased by 0.17°C. Although satellite observations over 1982–98 show a cooling over parts of the Antarctic continent, a general warming occurred in the surface temperature of the peripheral seas (Kwok and Comiso 2002). The latest aircraft and satellite laser-altimeter observations indicate an increased thinning of glaciers and accelerated rise of sea level from western Antarctica (Thomas et al. 2004). All these observations point to a general warming trend in the Southern Ocean, as in the other oceans of the world (Levitus et al. 2000, 2005).

Contrary to this warming trend, satellite passive microwave images display a significant increase in Ant-

Corresponding author address: Jinlun Zhang, Polar Science Center, Applied Physics Laboratory, College of Ocean and Fishery Sciences, University of Washington, Seattle, WA 98105.
E-mail: zhang@apl.washington.edu

DOI: 10.1175/JCLI4136.1

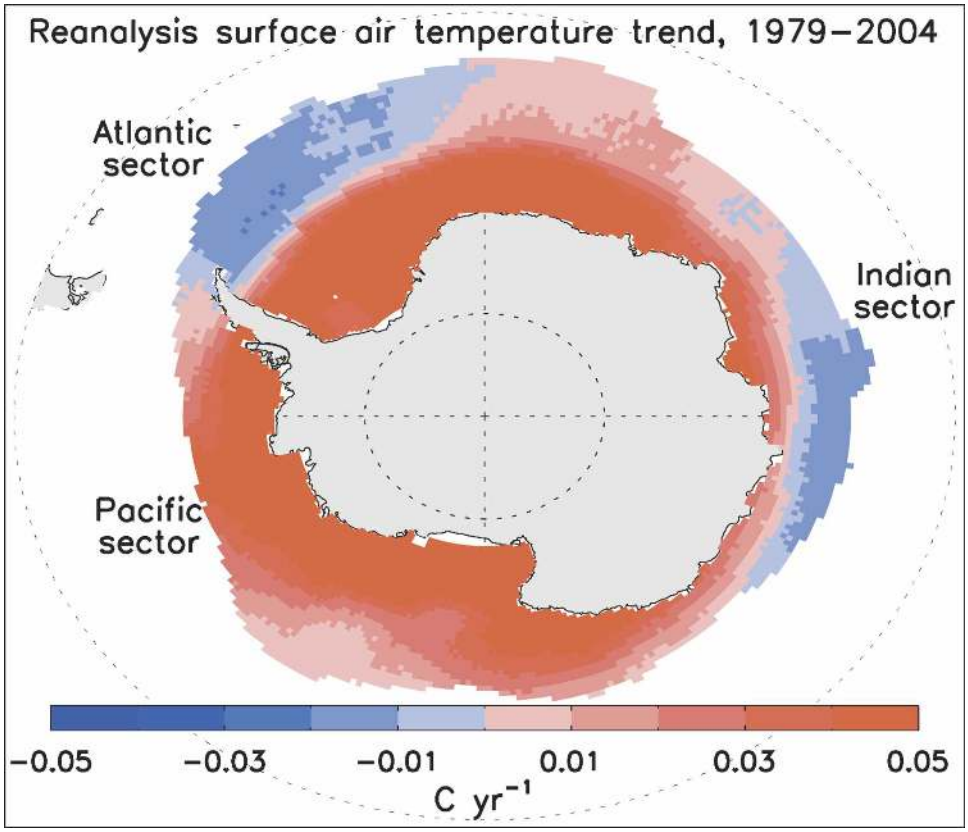

FIG. 1. Linear trend (1979–2004) of the NCEP–NCAR reanalysis surface air temperature over the ice-covered areas of the Southern Ocean defined as the 1979–2004 mean satellite-observed sea ice extent.

arctic sea ice concentration and extent since 1979 when quality space-based observations are available (Cavalieri and Parkinson 2003; Liu et al. 2004). The increase in the observed sea ice extent is 0.027×10^{12} m^2 yr^{-1} (0.22% yr^{-1}) during 1979–2004 (Fig. 2d; Table 1), based on the Hadley Centre global sea ice concentration data (HADISST; Rayner et al. 2003). This positive trend exceeds the 95% confidence level when tested by assuming that the regression residuals are statistically independent, but falls short of this confidence level when tested by accounting for temporal autocorrelation of the residuals (e.g., Wilks 1995; Santer et al. 2000). Whether the trend is at the 95% confidence level by no means diminishes the significance that the Antarctic sea ice has increased in an environment of prevailing warming during 1979–2004.

The variability and change of Antarctic sea ice are closely linked to the Southern Hemisphere Annular Mode (SAM; Thompson and Wallace 2000) and the well known El Niño–Southern Oscillation (ENSO). The ENSO describes an irregular cycle of warming and cooling of sea surface temperatures in the tropical Pacific Ocean, which has significant teleconnections with the Southern Ocean (e.g., Yuan and Martinson 2000). The SAM describes changes in the atmospheric circulation in the southern high latitudes. Positive polarities of the SAM generally lead to more ice in the eastern Ross–Amundsen sector and less ice in the Bellingshausen–northern Weddell sector, while the effect of the ENSO is the opposite (Liu et al. 2004). Over 1979−2002 the SAM index and the difference between the SAM and ENSO indices have shifted toward a more positive phase (Kwok and Comiso 2002), which seems to cause sea ice to increase in one sector and to decrease in another. However, they cannot explain the recent increase of sea ice in the Antarctic as a whole (Liu et al. 2004). On the other hand, an increase in precipitation may cause an increase in snow–ice formation because of an increase in snow depth, which may cause an increase in ice volume (Powell et al. 2005). Here the positive sea ice trend in a warming Southern Ocean is addressed using the coupled global Parallel

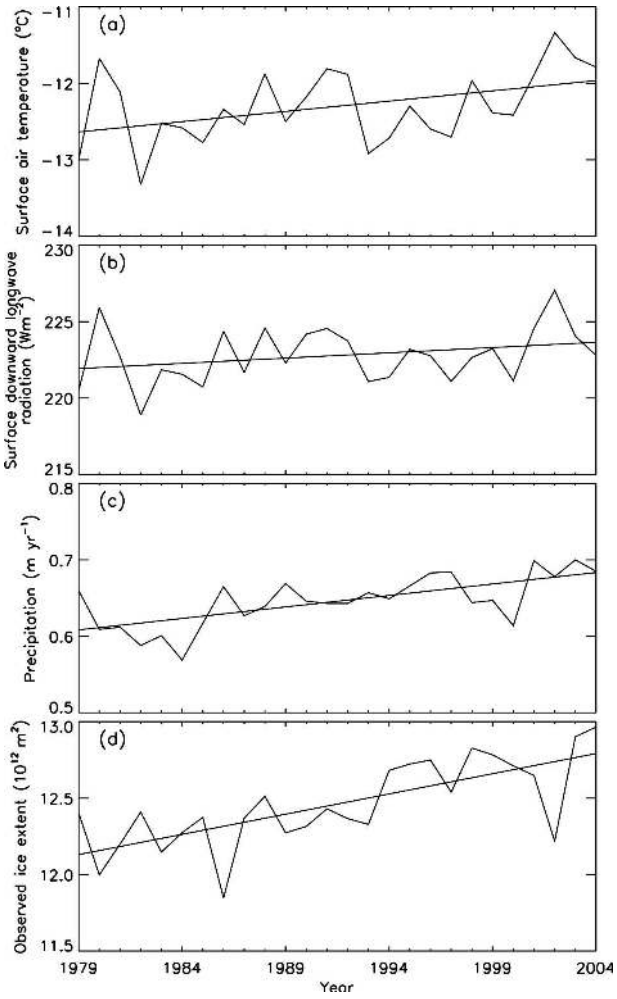

FIG. 2. Annual mean NCEP–NCAR reanalysis (a) SAT, (b) SDLR, and (c) P averaged over the ice-covered areas of the Southern Ocean, and (d) annual mean satellite-observed ice extent. Straight lines are trend lines.

Ocean and sea Ice Model (POIM; Zhang and Rothrock 2003) forced by the NCEP–NCAR reanalysis surface data.

2. Model description

The global POIM couples the Parallel Ocean Program (POP) developed at the Los Alamos National Laboratory (e.g., Smith et al. 1992) with a multicategory thickness and enthalpy distribution (TED) sea ice model (Zhang and Rothrock 2001; Hibler 1980). More model details can be found in Zhang and Rothrock (2003). For the purpose of analyzing model results, we give the conservation equation for ice thickness distribution (Hibler 1980):

$$\frac{\partial g}{\partial t} = -\nabla \cdot (\mathbf{u}g) - \frac{\partial (fg)}{\partial h} + \psi + F_L, \tag{1}$$

where g is the thickness distribution of sea ice (a normalized probability density function), $\mathbf{u}$ is the ice velocity, h is a coordinate variable describing the thickness of certain ice categories, f is the vertical ice growth rate due to the net surface heat flux, ψ is the redistribution function due to ridging, and F_L is the source term for ice melting from the ocean heat flux. The ocean heat flux used to melt ice F_L consists of the upward ocean heat transport provided to the surface ocean layer by the deeper layers F_{LO} and the portion of the surface heat flux that enters the surface ocean layer through leads and through the penetration of solar radiation through the ice F_{LS} (hereafter referred to as surface heat deposit). The heat absorbed in the surface ocean layer, $F_L = F_{\mathrm{LO}} + F_{\mathrm{LS}}$ does not factor in determining f but is allocated to melting ice (Hibler 1980). The first term on the right-hand side of (1) describes the change in thickness distribution due to ice advection; the second term on the right-hand side of (1) describes the change in thickness distribution due to ice growth (ice melt when $f < 0$) determined by the net surface heat flux. Overall, (1) states that a change in ice thickness distribution is due to a combination of ice advection, ice growth, ridging, and ocean heat flux–induced melting.

The conservation equation for the mean ice thickness or ice volume per unit area H can be derived from (1) such that

$$\Delta H = H_a + H_g - H_m, \tag{2}$$

where $H = \int_0^\infty ghdh$, ΔH is the change in ice thickness, $H_a = -\nabla \cdot (\mathbf{u}H)\,(\Delta t)$ describes the change due to local ice advection, $H_g = \int_0^\infty fgdh(\Delta t)$ the change due to local ice growth, and $H_m = -\int_0^\infty F_L hdh(\Delta t)$ the change due to local ice melting from the ocean heat flux. Because ridging only transfers ice from one category to another, it does not contribute to the change in mean ice thickness. The ocean heat flux–induced melting H_m consists of two parts, H_{mo} and H_{ms}, corresponding to F_{LO} and F_{LS}. If we integrate (2) over a sufficiently large area that includes all the possible ice-covered areas of the Southern Ocean, we obtain the conservation equation for the total volume V of Antarctic sea ice such that

$$\Delta V = G - M, \tag{3}$$

where ΔV is the change in total ice volume, G is the total ice growth due to the net surface heat flux, and M is the total melting from ocean heat flux. The local ice advection term H_a in (2) does not contribute to the change in total ice volume in (3). Again, the total melting from ocean heat flux M consists of two parts:

$$M = M_o + M_s, \tag{4}$$

TABLE 1. 1979–2004 mean and linear trend for some variables of reanalysis data, satellite observations, and model simulation results with (without) interannual variability of precipitation (the case with snow–ice formation is not included). The SAT, SDLR and SDSR, *P*, snow depth, and ocean temperature, salinity, and density are averaged over the ice-covered areas defined as the 1979–2004 mean satellite-observed sea ice extent. Bold numbers exceed the 95% confidence level when tested in a way that accounts for temporal autocorrelation.

	Mean	Trend	Trend/ |mean| × 100%	Unit of trend
Reanalysis SAT	−12.30	**0.027**	0.22	°C yr^{-1}
Reanalysis SDLR	222.8	0.069	0.03	W m^{-2} yr^{-1}
Reanalysis SDSR	126.6	**−0.047**	0.04	W m^{-2} yr^{-1}
Reanalysis *P*	0.65	**0.003**	0.46	m yr^{-1}
Satellite-observed ice extent	12.46	0.027	0.22	10^{12} m^2 yr^{-1}
Simulated ice extent	13.83 (13.88)	0.084 (0.043)	0.61 (0.31)	10^{12} m^2 yr^{-1}
Simulated total ice volume	20.25 (20.30)	0.201 (0.130)	1.0 (0.6)	10^{12} m^3 yr^{-1}
Simulated total ice growth	809.60 (808.14)	**−2.383 (−1.460)**	−0.29 (−0.18)	10^{12} m^3 yr^{-2}
Simulated total melting from ocean heat flux	809.39 (808.10)	**−2.397 (−1.468)**	−0.30 (−0.18)	10^{12} m^3 yr^{-2}
Simulated total net ice production	0.069 (0.046)	0.014 (0.008)	20.4 (17.6)	10^{12} m^3 yr^{-2}
Simulated snow depth	0.43 (0.42)	**0.010 (0.006)**	2.3 (1.4)	m yr^{-1}
Simulated total upward ocean heat transport	307.53 (306.12)	−1.223 (−0.390)	−0.40 (−0.13)	10^{12} m^3 yr^{-2}
Simulated total surface heat deposit	501.86 (501.98)	**−1.174 (−1.077)**	−0.23 (−0.21)	10^{12} m^3 yr^{-2}
Simulated ocean salinity in upper 200 m	34.525 (34.524)	−0.003 (0.001)	−0.009 (0.003)	psu $decade^{-1}$
Simulated ocean temperature in upper 200 m	−0.999 (−0.978)	**0.007 (0.006)**	0.70 (0.61)	°C yr^{-1}
Simulated ocean density in upper 200 m	27.765 (27.763)	−0.005 (−0.002)	−0.018 (−0.007)	kg m^{-3} $decade^{-1}$

where M_o is the amount of ice melted by the total upward ocean heat transport and M_s by the total surface heat deposit.

Accompanying the TED sea ice model is a model of snow thickness distribution g_s, corresponding to the ice thickness distribution g. The snow conservation equation and the treatment of the snow thickness distribution are given by Flato and Hibler (1995, see their appendix).

The global POIM grid configuration is similar to that used by Zhang and Rothrock (2003). It is based on a generalized orthogonal curvilinear coordinate system. In the Northern Hemisphere the model grid is a gradually stretched curvilinear coordinate grid with the northern grid pole displaced into Greenland. In the Southern Hemisphere the model grid is a regular spherical coordinate grid. The horizontal dimension is 360 × 276 with a resolution of ⟨0.65°⟩ (angle brackets denote the average resolution of surface ocean points).

The model is driven by daily varying NCEP–NCAR reanalysis forcing fields, including 10-m winds, SAT, specific humidity, surface downward shortwave radiation (SDSR), SDLR, precipitation (*P*), and evaporation (*E*). Changes in SAT, SDLR, and *P* over 1979–2004 are shown in Figs. 1 and 2 and Table 1. Also shown in Table 1 is the negative trend in the reanalysis SDSR, which reflects the effect of a warming atmosphere that increases evaporation and condensation and therefore cloudiness. The annual mean and trend of the SDSR are smaller in magnitude than the SDLR (Table 1). There are many uncertainties associated with the reanalysis forcing, but the forcing represents an atmospheric warming scenario, which, when used to drive the model, leads to a simulation of an increased Antarctic sea ice cover. Therefore, the forcing is ideal for this study.

Model spinup consists of an integration of 30 yr using 1948 forcing fields repeatedly. The spinup allows the model to approach an approximate steady state such that the differences between the mean ocean temperatures and salinities, averaged over the upper 200 m of the Southern Ocean, of the last two spinup years are 0.007°C and 0.0004 psu. After this spinup the model proceeds to simulate the period 1948–2004. The standard simulation does not include model parameterization of snow–ice formation due to seawater flooding and freezing at the snow–ice interface. To examine the effect of snow–ice formation, a sensitivity run is conducted in which snow–ice formation is parameterized following Powell et al. (2005). To isolate the effect of increasing *P* on an increasing Antarctic sea ice cover, a second sensitivity run is also conducted, which is a model integration using the same reanalysis forcing except that the *P* and *E* are from daily climatology. The daily climatology is created by averaging *P* and *E* over 1979–2004 so that there is no interannual variability. To test the model's sensitivity to initial conditions, a third sensitivity run is conducted using different initial sea ice and ocean conditions. Results from the third sensitivity run are not shown here, but they indicate that the model using different initial conditions converges to essentially the same solution for sea ice and the upper

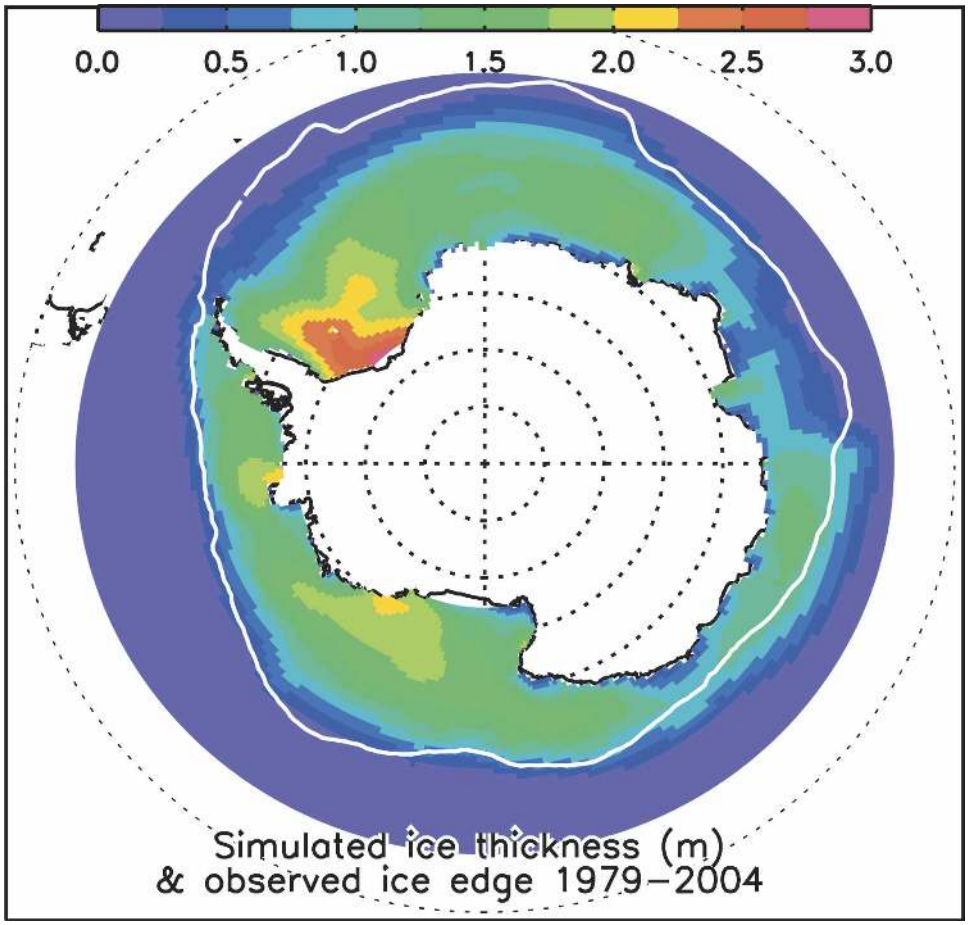

FIG. 3. 1979–2004 mean model-simulated ice thickness and satellite-observed ice extent. The white line represents the satellite-observed ice edge with 0.15 ice concentration.

ocean after about 10 yr of spinup. Results from the standard simulation and the first two sensitivity runs are presented here. To distinguish the different model integrations, the standard simulation is referred to as the case with "interannually varying P without snow–ice formation," the first sensitivity run "interannually varying P with snow–ice formation," and the second sensitivity run "climatological P without snow–ice formation." The presented results are mainly from the standard simulation, unless stated otherwise.

3. Model results and observations

a. Increasing sea ice volume

The simulated ice thickness (H) and the satellite-observed ice extent (HADISST) are shown in Fig. 3. The model reasonably captures the observed ice extent, except that it underestimates (overestimates) ice extent in the Atlantic sector (part of the Indian sector). The simulated long-term mean spatial pattern is that ice thickness is generally below 1.5 m in most regions of the Southern Ocean, which is consistent with observations (Wadhams et al. 1987; Jeffries et al. 2001). Thicker ice (>2 m) mainly concentrates in the western Weddell Sea and in part of the Pacific sector. Compared with submarine observations of arctic ice draft (Rothrock et al. 1999), Antarctic sea ice is significantly thinner than its arctic counterpart. The thinner Antarctic ice cover may be due to a less stratified Southern Ocean; considerably more ocean heat flux is generated than in the Arctic Ocean (McPhee et al. 1999; Maykut and McPhee 1995).

The simulated ice thickness (H) increases from 1979 to 2004 in most of the ice-covered areas in the Southern Ocean (defined hereafter as the 1979–2004 mean satellite-observed sea ice extent shown in Fig. 3). This is also illustrated in the spatial distributions of the simulated ice concentration trends during that period (Figs. 4a,b). The linear trend (a least squares fit) of the observed ice

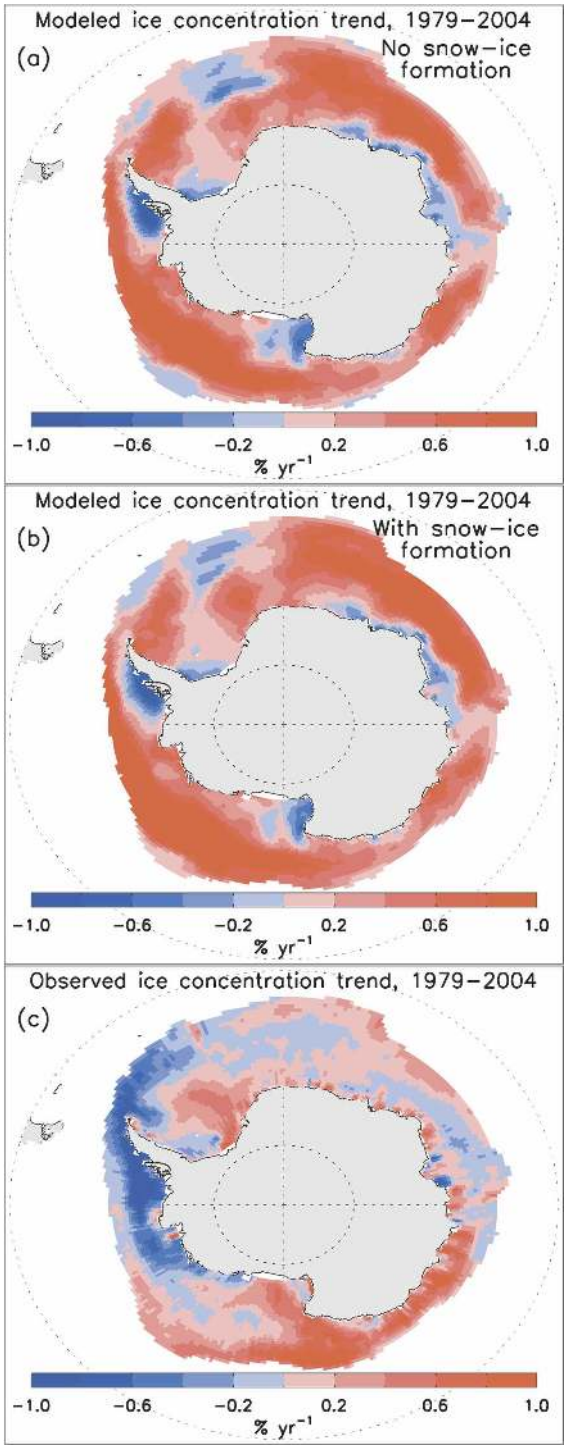

FIG. 4. Linear trends (1979–2004) of (a), (b) model-simulated mean annual ice concentration and (c) satellite-observed mean annual ice concentration.

concentration also shows an increase in sea ice in most of the ice-covered areas (Fig. 4c). Compared with the observations, the model overestimates the areas of increasing sea ice in the Atlantic and Pacific sectors, but it performs better in the Indian sector. The model agrees with observations in showing an increased ice cover in most of the Ross Sea (Parkinson 2002). However, off part of the Ross Sea coast the model simulates decreasing sea ice in disagreement with the observations, which is certainly due to the uncertainties in the model and the forcing. Off Adelaide Island and part of the Weddell Sea coast the model simulates decreasing sea ice in agreement with the observations.

Table 1 shows that the simulated total volume (V) of Antarctic sea ice has a positive trend of 0.20×10^{12} m^3 yr^{-1} over 1979 to 2004. The total ice volume increases particularly faster from 1982 to 1987 and actually decreases from 1994 to 2000 (Fig. 5a). This emphasizes the dependence of the trend on the time period for which the trend is calculated when there is long-term variability. Compared to the satellite observations, the model overestimates the mean and variability of ice extent (Fig. 5b; Table 1). Like the positive trend of the observed sea ice extent, the positive trend of the simulated total sea ice volume and ice extent over the whole period of 1979–2004 is above the 95% confidence level with a more liberal testing method, but is below the 95% confidence level with a more stringent testing method that accounts for the effect of autocorrelation (e.g., Wilks 1995; Santer et al. 2000). The significance tests of those trends listed in Table 1 are all based on the more stringent test method. Using climatological P does not significantly change the ice volume or extent. As expected, the model creates more ice by allowing snow–ice formation. However, since the reanalysis P is much larger than satellite observations in the Antarctic (Powell et al. 2005), the magnitude of the simulated total ice volume or ice extent (or other quantities shown later) should fall in between those with and without snow–ice formation if less biased P is used.

b. Decreasing ice growth and melt

As described by (2), the change in ice thickness (H) is due to local ice advection (H_a), ice growth (H_g), and ice melting from ocean heat flux (H_m). The simulated local ice growth is mostly positive in the Southern Ocean except in a small area in the Indian sector (Fig. 6a); the simulated ice melting from ocean heat flux is positive everywhere, as expected (Fig. 6b). Their difference, the net ice production ($H_g - H_m$), is negative in most of the ice-covered areas except along the coast of Antarctica and in part of the Weddell and Ross Seas where ice production can be rather high (Fig. 6c). In other words, the coastline areas of Antarctica are a major "factory" of sea ice, according to the model. The reason is that the ice–ocean dynamics of the model tend

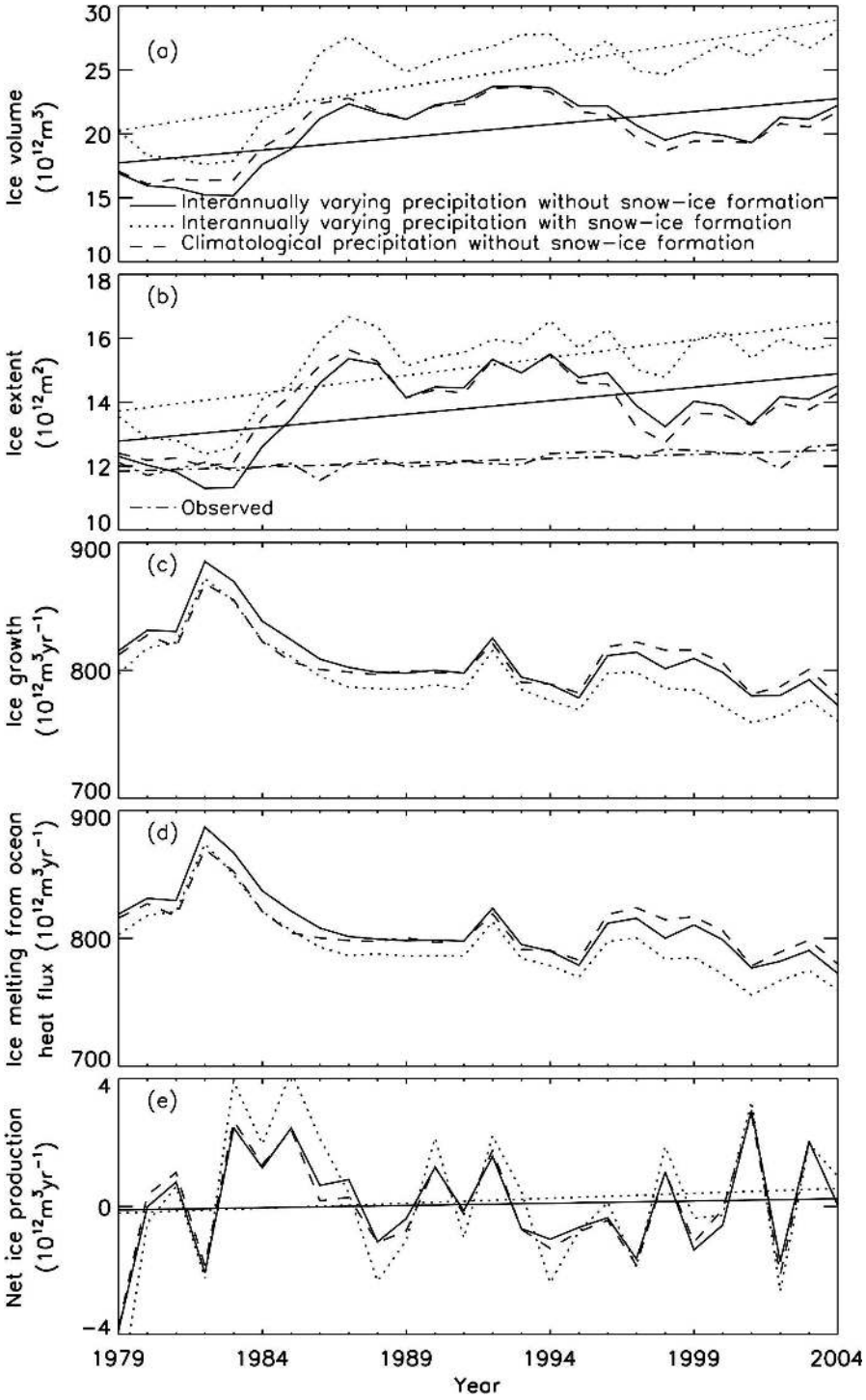

FIG. 5. Simulated (a) total volume of sea ice, (b) total ice extent, (c) total ice growth, (d) total ice melting from ocean heat flux, and (e) total net ice production for the Southern Ocean.

to move ice to the open ocean from the coast and part of the Weddell and Ross Seas, owing to the advection processes (Fig. 6d), thus providing ice to the open ocean for widespread melting and at the same time creating opening along the coast and part of the Weddell and Ross Seas where vigorous growth is possible. Ice–ocean dynamical processes are important in shaping the spatial distribution and therefore general be-

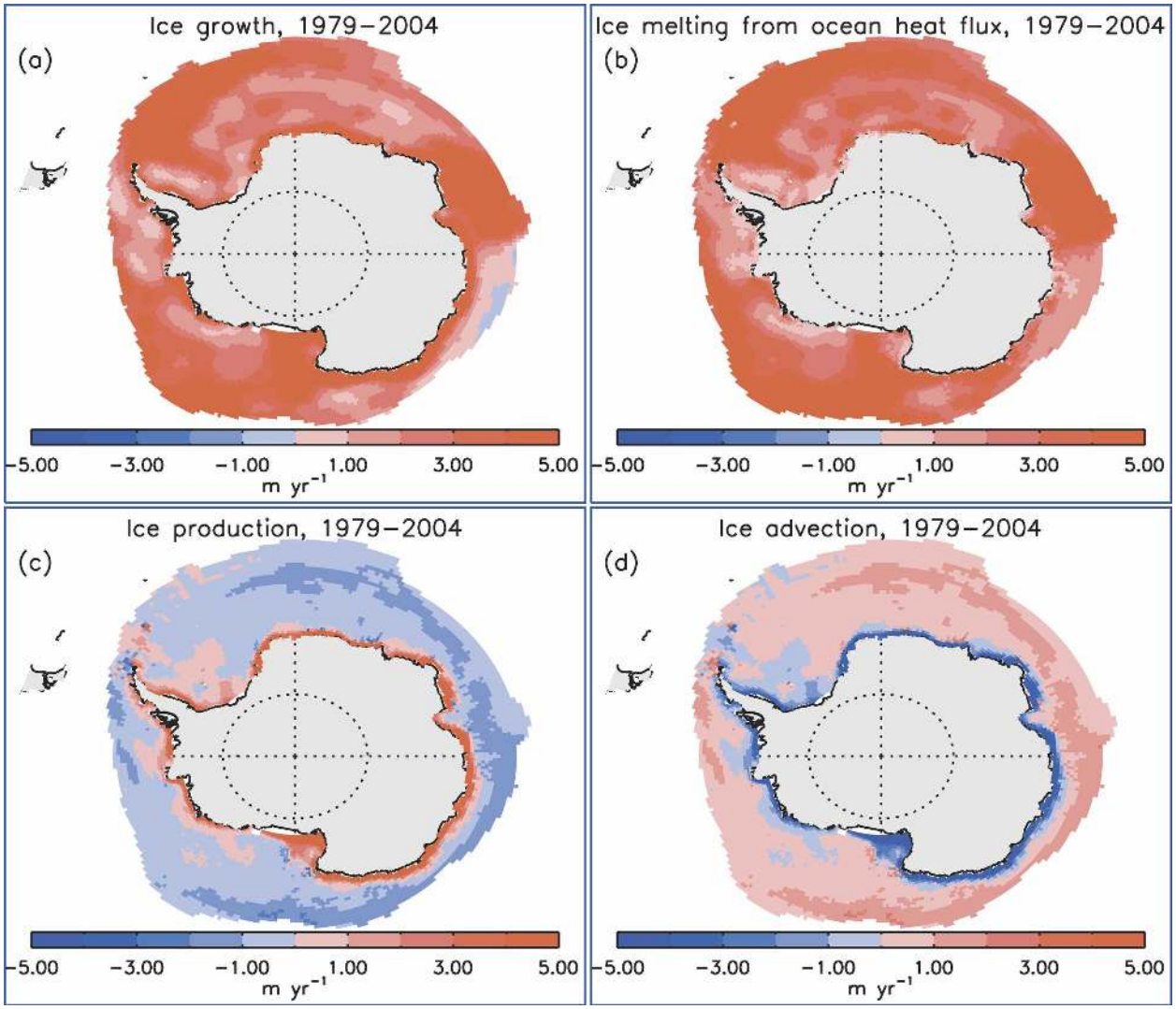

FIG. 6. Simulated 1979–2004 (a) mean ice growth, (b) ice melting from the ocean heat flux, (c) net ice production, and (d) ice advection over the ice-covered areas of the Southern Ocean.

havior of ice advection, growth, and melting. But because ice advection (H_a) makes no direct contribution to the change in the total Antarctic sea ice volume (V) in (3), the important role of ice advection is "behind the scenes." According to (3), the total ice volume is controlled by the total ice growth (G) and the total ice melting from the ocean heat flux (M).

The simulated total ice growth (G) decreases from 1979 to 2004 for all three cases (Fig. 5c). This is also reflected in the linear trends of local ice growth H_g, which are mostly negative in the ice-covered areas (Fig. 7a). The downward trend of total ice growth is due to the increase in SAT and SDLR as well as in the ice mass (Figs. 2a and 5a). The simulated total ice growth is reasonably correlated, negatively, with SAT ($R = -0.47$; Table 2). For example, the total ice growth reaches the maximum in 1982 when SAT drops to the minimum. The total ice growth is even more strongly correlated, negatively, with the total ice volume ($R = -0.73$; Table 2). This is because the vertical ice growth rates (f) decrease rapidly for ice with thickness less than 1 m (Maykut 1986) and the simulated ice thickness in the Southern Ocean is mostly less than 1.5 m (Fig. 3), which explains the strong negative correlation between the total ice growth and the total ice volume.

The simulated total ice melting from ocean heat flux (M) decreases in the same manner as the total ice growth (Figs. 5c,d). This is also reflected in the similar spatial patterns of the linear trends of H_g and H_m (Figs. 7a,b). The total ice melting from ocean heat flux and

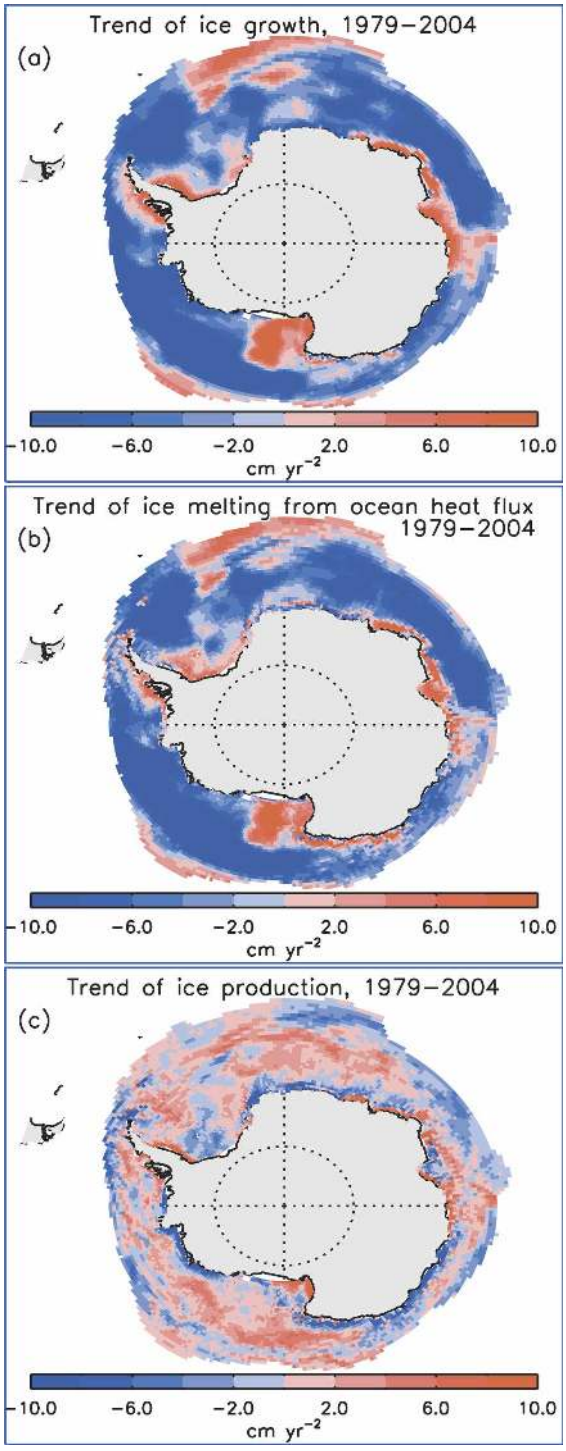

FIG. 7. Linear trends (1979–2004) of (a) simulated ice growth, (b) ice melting from the ocean heat flux, and (c) net ice production.

the total ice growth are almost perfectly correlated ($R = 0.99$; Table 2). However, because H_m often decreases more rapidly than H_g, the local net ice production $H_g - H_m$ has a positive trend in most ice-covered areas (Fig. 7c), leading to an increase of 0.014×10^{12} m^3 yr^{-2} in the total net ice production (Table 1; Fig. 5e). The increase in modeled Antarctic sea ice is due to total ice melting from the ocean heat flux decreasing more rapidly than the total ice growth, resulting in a net increase in ice production and mean ice thickness during 1979–2004. This appears to be true in all three cases considered, whether P climatology or the parameterization of snow–ice formation is used in the model.

c. *Increasing ocean stratification and decreasing upward ocean heat transport*

The decrease in the total ice melting from ocean heat flux from 1979 to 2004 is due to the decrease in either the total upward ocean heat transport M_o or the total surface heat deposit M_s (Figs. 8a,b; Table 1). The decrease in the total surface heat deposit is related to the increase in ice thickness and compactness that tends to reduce the penetration of surface heat flux through leads and bare ice. The local surface heat deposit $H_{\rm ms}$ increases (Fig. 9b) mainly in the areas where ice concentration decreases (Figs. 4a,b). The spatial pattern of the $H_{\rm mo}$ linear trends (Fig. 9a) is close to that of H_m. (Fig. 7b). This is why the total upward ocean heat transport and the total ocean heat flux are closely correlated ($R = 0.83$; Table 2), with significant downward trend during 1979–2004 (Table 1). This downward trend is greater than that of the total surface heat deposit, which indicates that the decreasing upward ocean heat transport may play a more prominent role in increasing the Antarctic sea ice.

The upward ocean heat transport is generated by oceanic advection, diffusion, and convective overturning. In an ice-covered area in the Arctic, convective overturning is the major contributor to the upward ocean heat transport (Zhang 1993). In the Southern Ocean, convection occurs along the continental shelves of Antarctica as well as in the open ocean owing to ice formation and associated salt rejection (Martinson et al. 1981; Baines and Condie 1998). Bitz et al. (2006) have demonstrated the strong influence of sea ice on convection and the upward ocean heat transport through freshwater transport, which makes the surface waters more stable in a greenhouse warming scenario. Because the Southern Ocean is generally less stratified than the Arctic Ocean (Deacon 1977), convective overturning is likely to play a more prominent role in determining the magnitude of the upward ocean heat transport. That is, the upward heat transport, or equivalently the amount of ice melted by it (M_o), is a proxy of the ocean's water column stability. The simulated mean ocean density (σ_θ) in the upper 200-m ocean layer decreases slightly during 1979–2004 (Fig. 8c), indicating a

TABLE 2. Correlations (R) among simulated annual mean total ice volume, ice growth, ice melting from ocean heat flux, upward ocean heat transport, surface heat deposit, and ocean temperature and density (σ_θ) in the upper 200 m of the ocean, and annual mean reanalysis SAT and SDLR. The SAT, SDLR, and the ocean temperature and density are averaged over the ice-covered areas defined as the 1979–2004 mean satellite-observed sea ice extent.

	SDLR	Ice volume	Ice growth	Ice melting from ocean heat flux	Upward ocean heat transport	Surface heat deposit	Ocean temperature in upper 200 m	Ocean density in upper 200 m
SAT	0.90	0.22	−0.47	−0.49	−0.49	−0.09	0.39	−0.44
SDLR		0.25	−0.44	−0.46	−0.51	0.02	0.22	−0.40
Ice volume			−0.73	−0.73	−0.76	−0.07	0.39	−0.60
Ice growth				0.99	0.82	0.45	−0.57	0.59
Ice melting from ocean heat flux					0.83	0.43	−0.57	0.59
Upward ocean heat transport						−0.14	−0.31	0.68
Surface heat deposit							−0.51	−0.06
Ocean temperature, upper 200 m								−0.57

strengthening of ocean stratification. This is because the model creates a decrease in ocean density in the upper 200 m in most of the Atlantic and Pacific sectors (Fig. 9c). The strengthened stratification is likely to suppress convective overturning, thus reducing the total upward ocean heat transport (Fig. 8a). The ocean density in the upper 200 m and the total upward heat transport are correlated ($R = 0.68$; Table 2).

The simulated ocean density in the upper 200 m decreases because the ocean salinity decreases while the ocean temperature increases in the same layer (Figs. 8d,e; Table 1). The temporal and spatial patterns of the ocean density resemble those of the salinity (Figs. 8c,d and 9c,d), owing to the fact that the density of seawater is primarily controlled by salinity in ice-covered areas of the Southern Ocean. The ocean temperature in the upper 200 m increases in most ice-covered areas (Fig. 9e) because the increasing SAT tends to warm the upper ocean in, mainly, the summer when the Southern Ocean is largely ice free. Although there is no spatial one-to-one correspondence between the warming SAT and the warming upper ocean, the averaged SAT and ocean temperature in the upper 200 m over the ice-covered areas are somewhat correlated ($R = 0.39$; Table 2).

When snow–ice formation is incorporated in the model, the simulated upper ocean becomes warmer and fresher. This is because of enhanced heat insulation by an increased ice cover and the partial melting of snow-converted ice in the upper ocean. As a result, the ocean is more stratified and the upward ocean heat transport is reduced. However, the variability and trend of these related quantities are similar to those from the standard simulation without incorporating the snow–ice formation.

The key to increasing Antarctic sea ice in warming conditions both above and below is the steeper decrease in ice melting from ocean heat flux than in ice growth. This requires that any decrease in ice growth and hence in salt rejection suppresses convective overturning activities in such a way as to significantly reduce the heat brought up mainly by the overturning processes. For this to happen the magnitude and variation of the ocean heat flux responsible for ice melting (H_m) must be comparable to or even greater than the net surface heat flux responsible for ice growth (H_g) in a sufficiently large area so that the changes in ice melting may have a chance to dominate those in ice growth. This condition is possible in the ice-covered areas of the Southern Ocean where the ocean is weakly stratified and has a relatively large ocean heat flux (McPhee et al. 1999). The model reflects this condition by creating negative net ice production ($H_g - H_m$) in most of the Antarctic open ocean (Fig. 6c).

d. The role of increasing precipitation

The reanalysis P increases with the increasing SAT during 1979–2004 (Fig. 2c; Table 1). To examine the role of increasing P on increasing Antarctic sea ice, a second sensitivity run is conducted with the model forced by climatological P and E (section 2).

When the climatological P (no interannual variability) is used to force the model, the simulated total ice volume increases from 1979 to 2004, although to a lesser degree than when the normal NCEP–NCAR reanalysis P forcing is used (Fig. 5a; Table 1). This indicates that the increasing P is not the main cause of the simulated increase of Antarctic sea ice cover. Like the standard model run, the second sensitivity run simulates decreasing ice growth and ice melting from the ocean heat flux; the decrease in ice melting is steeper. Thus, the sensitivity run creates an increase in the total net ice production and therefore in the total ice volume (Table 1), meaning that the primary cause of the in-

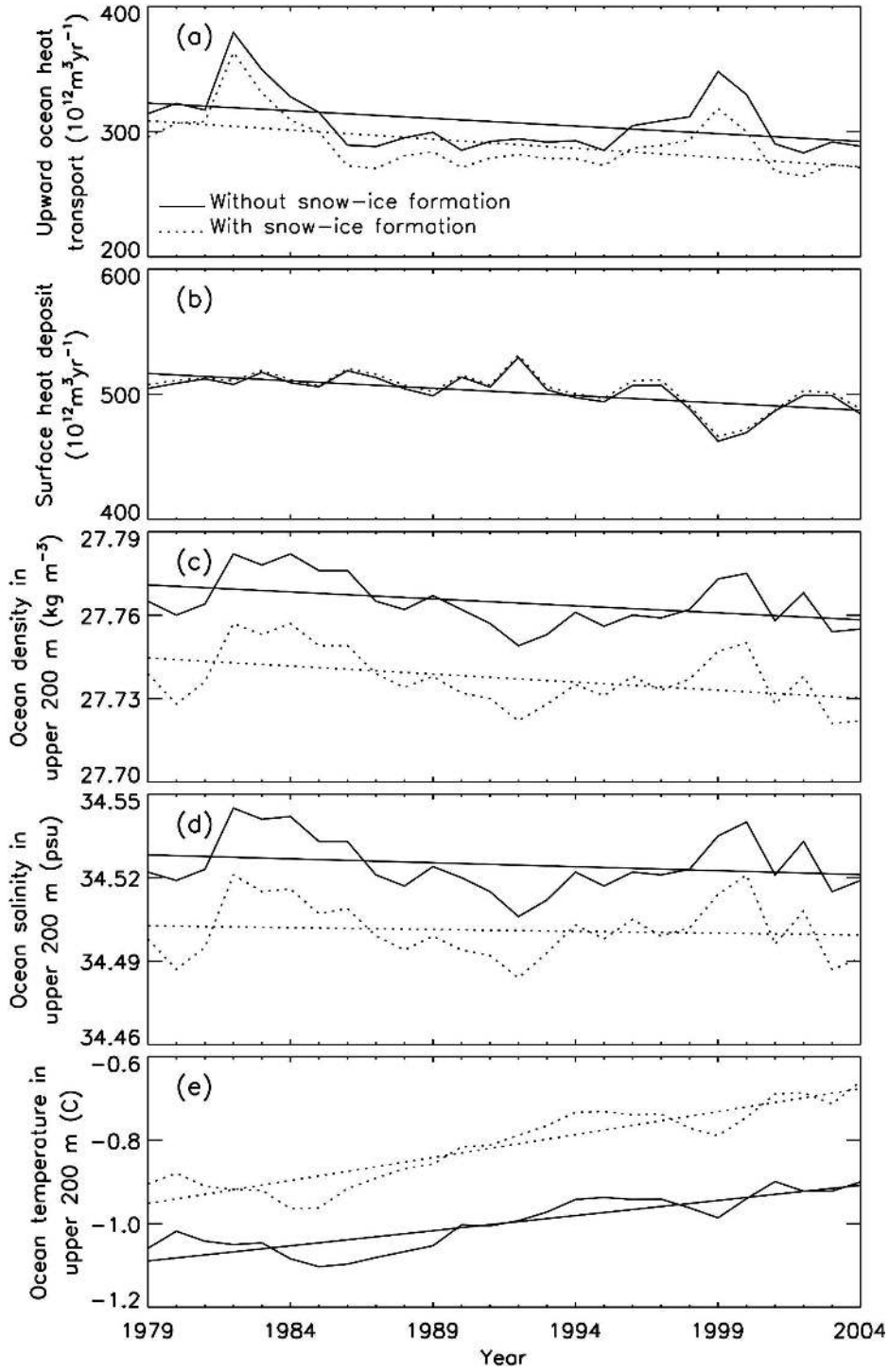

FIG. 8. Simulated (a) total upward ocean heat transport and (b) surface heat deposit for the Southern Ocean, and simulated (c) ocean density, (d) salinity, and (e) temperature in the upper 200-m ocean layer averaged over the ice-covered areas of the Southern Ocean.

creasing Antarctic sea ice is the steeper decrease in ocean heat flux, regardless of *P*.

An increase in the net ice production increases the salinity in the upper ocean; salinity in the upper 200 m simulated by the sensitivity run has a positive trend (Table 1). However, because ocean temperature in the upper 200 m simulated by the sensitivity run increases at a slightly faster pace, the average density of the sea-

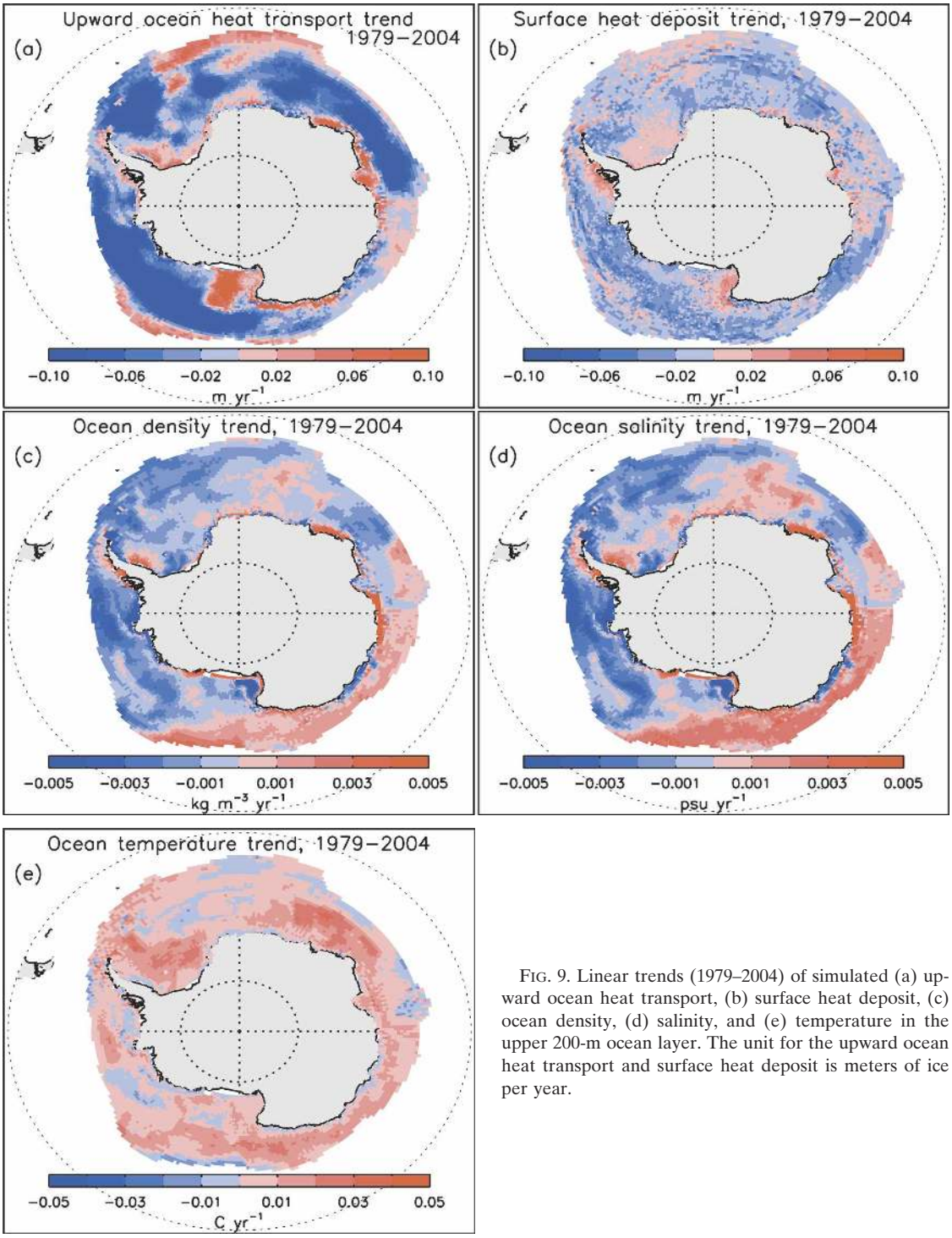

FIG. 9. Linear trends (1979–2004) of simulated (a) upward ocean heat transport, (b) surface heat deposit, (c) ocean density, (d) salinity, and (e) temperature in the upper 200-m ocean layer. The unit for the upward ocean heat transport and surface heat deposit is meters of ice per year.

water in the layer still decreases, leading to an increase in the stratification of the upper ocean and therefore a decrease in ocean heat flux. When P increases, on the other hand, the ocean salinity in the upper 200 m simulated by the standard model run has a negative trend. This, combined with the increasing ocean temperature in that layer, leads to a stronger stratification in the upper ocean and a steeper decrease in the ocean heat flux. This is why the total net ice production and hence the total ice volume simulated by the standard model

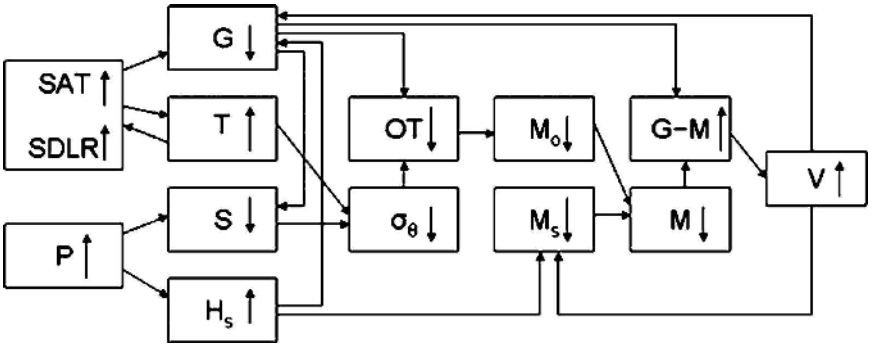

FIG. 10. Illustration of a mechanism that explains the possibility of an increasing Antarctic sea ice cover in a warming environment. Air–sea interaction (between SAT and upper-ocean temperature T) is also illustrated. SDLR represents surface downward longwave radiation, P is precipitation, G is the ice growth rate, S is the upper-ocean salinity, H_s is the snow depth, OT is the convective overturning, σ_θ is the upper-ocean density, M_o is the amount of ice melted by the upward ocean heat transport, M_s is the surface heat deposit, M is the sum of M_o and M_s, and V is the ice volume. The upward (downward) arrow inside a box represents an increase (decrease); the direction of the other arrows represents cause and effect. For example, an increase in SAT causes a decrease in ice growth.

run increases slightly faster than those simulated by the sensitivity run (Fig. 5a; Table 1).

4. Concluding remarks

To investigate the seeming paradox of increasing Antarctic sea ice and increasing atmospheric and oceanic temperatures for the Southern Ocean during 1979–2004, a global POIM that includes a POP ocean model and a multicategory TED sea ice model was forced by the NCEP–NCAR reanalysis data that include increasing SAT, SDLR, and P and decreasing SDSR. There are many uncertainties with both the model and the reanalysis data, and the results must be viewed with caution. Driven by the reanalysis forcing, the model simulates an increase of 0.20×10^{12} m^3 yr^{-1} (1.0% yr^{-1}) in total Antarctic sea ice volume and 0.084×10^{12} m^2 yr^{-1} (0.6% yr^{-1}) in sea ice extent from 1979 to 2004, whereas the satellite observations show an increase of 0.027×10^{12} m^2 yr^{-1} (0.2% yr^{-1}) in sea ice extent during the same period (Figs. 2d and 5a; Table 1). When snow–ice formation is parameterized in the model, the simulated positive trend is even larger. This indicates that it is possible for the Antarctic sea ice to increase significantly in warming atmospheric conditions.

The nature of the phenomenon of increasing Antarctic sea ice in a warming environment may be explained by the following (Fig. 10). When SAT/SDLR increases, the upper-ocean temperature increases (which causes SAT to increase concurrently through air–sea interactions) and ice growth decreases, leading to a decrease in salt rejection from the new ice and therefore in the upper-ocean salinity. The increase in ocean temperature and the decrease in ocean salinity result in a decrease in water density in the upper ocean, leading, in conjunction with reduced salt rejection, to enhanced thermohaline stratification and weakened convective overturning. Weakened overturning in turn reduces the upward ocean heat transport, leading to reduced ocean heat flux available to melt sea ice. The ocean heat flux–induced ice melting decreases faster than the ice growth in the weakly stratified Southern Ocean, which allows for a large variation of the ocean heat flux, leading to an increase in the net ice production and hence ice mass. Thus, this study has identified a possible mechanism that explains the increasing trend in Antarctic sea ice under warming conditions. Note, however, that there may be other mechanisms that can be used to explain the paradox.

The second sensitivity run using P climatology without interannual variability also results in an increase in Antarctic sea ice from 1979 to 2004. This indicates that the increasing reanalysis P used in the other two model runs is not the main reason behind the simulation of increasing sea ice. The main reason is that the sensitivity run still reduces the ice melting from the ocean heat flux more dramatically than ice growth by increasing the ocean's stratification through thermal effects, which leads to decreasing convective overturning, though to a lesser degree than when the increasing P is used. An increasing P in the model tends to further reduce ice growth by increasing the snow depth (Table 1; Fig. 10). An increasing P also tends to reduce the upper-ocean salinity and density, leading to further reduced convec-

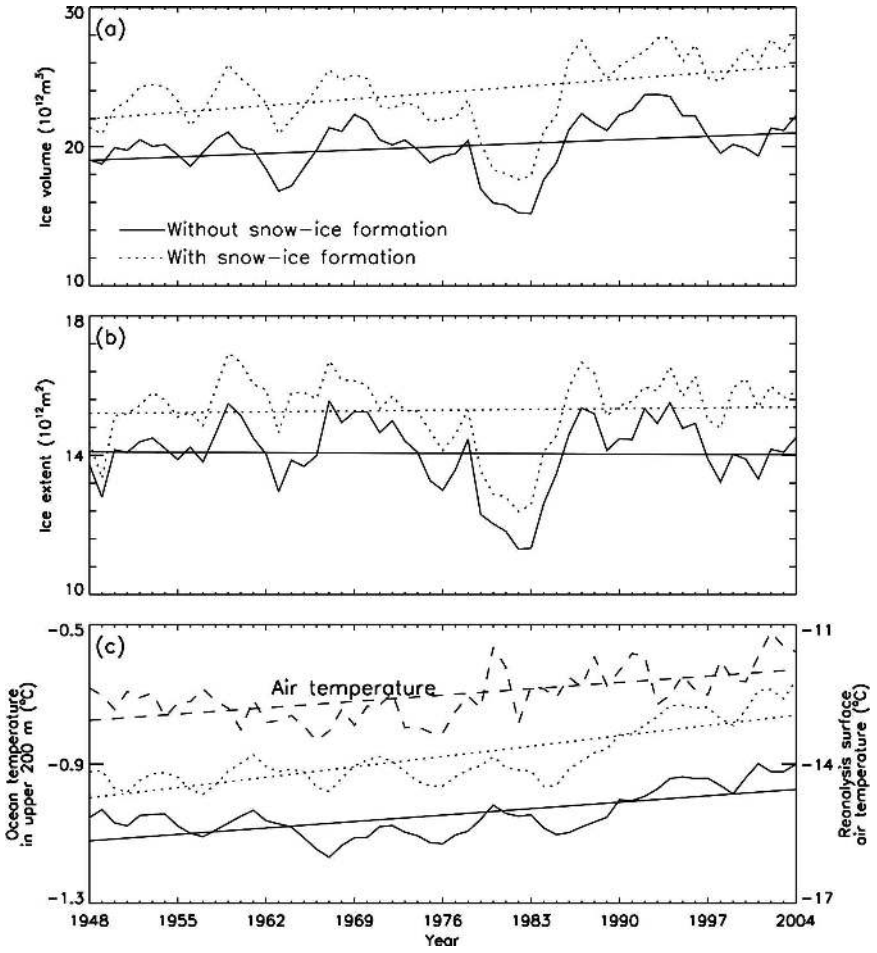

FIG. 11. Simulated total Antarctic (a) sea ice volume, (b) extent, and (c) ocean temperature in the upper 200-m ocean layer (with reanalysis surface air temperature) over 1948–2004.

tive overturning and the associated upward heat transport. This is why the model forced by the reanalysis P with a positive trend creates slightly more ice than the sensitivity run forced by P climatology. Note that the increasing P causes the ice volume to increase more when snow–ice formation is parameterized.

The simulated ice volume has a generally positive trend over the whole period of 1979–2004, but it increases more noticeably from 1982 to 1987, owing to a rapid decrease in the upward ocean heat transport, and decreases significantly from 1994 to 2000, owing to a rapid increase in the upward ocean heat transport (Figs. 5a and 8a). This behavior stresses the importance of ocean processes in determining the budget of Antarctic sea ice, and also indicates that changes in the upward ocean heat transport may cause rapid or abrupt changes in the Antarctic sea ice extent. Furthermore, the simulated ice volume decreases from 1994 to 2000 when the reanalysis SAT increases during that period (Fig. 2a). This is due to an increase in the upward ocean heat transport in the late 1990s and early 2000s.

The ice advection term H_a does not appear in (3); this by no means diminishes the importance of the horizontal advective processes (meridional and circumpolar) both in the ice cover and in the ocean. Region-dependent horizontal advective processes play a key role in redistributing heat and mass, and therefore contribute to the overall behavior of the Antarctic ice–ocean system.

Finally, it is necessary to point out that so far we have only focused on the satellite era of 1979–2004 during which both the model and observations show an increasing Antarctic sea ice cover under warming conditions in both the atmosphere and the ocean. This appears to be also true over the period 1948–2004 according to the model (Fig. 11). Although the model-simulated Antarctic sea ice extent stays flat, the simulated total sea ice volume increases over 1948–2004

(in agreement with Fichefet et al. 2003) when both the reanalysis surface air temperature and the simulated upper-ocean temperature have a positive trend.

Acknowledgments. The author is grateful for the support of NASA (Grant NNG04GB03G) and NSF (Grant OPP-0240916), and thanks R. W. Lindsay and M. Steele for constructive comments, and A. Schweiger and M. Ortmeyer for computer assistance.

REFERENCES

Alley, R. B., and Coauthors, 2003: Abrupt climate change. *Science,* **299,** 2005–2010.

Baines, P. G., and S. Condie, 1998: Observations and modelling of Antarctic downslope flows: A review. *Ocean, Ice and Atmosphere: Interactions at the Antarctic Continental Margin,* S. S. Jacobs and R. Weiss, Eds., AGU Antarctic Research Series, Vol. 75, Amer. Geophys. Union, 29–49.

Bitz, C. M., P. R. Gent, R. A. Woodgate, M. M. Holland, and R. Lindsay, 2006: The influence of sea ice on ocean heat uptake in response to increasing CO_2. *J. Climate,* **19,** 2437–2450.

Cavalieri, D. J., and C. L. Parkinson, 2003: 30-year satellite record reveals contrasting Arctic and Antarctic decadal sea ice variability. *Geophys. Res. Lett.,* **30,** 1970, doi:10.1029/2003GL018031.

Deacon, G. E. R., 1977: Antarctic water masses and circulation. *Polar Oceans,* M. J. Dunbar, Ed., Institute of North America, 11–16.

Fichefet, T., H. Goosse, and M. A. M. Maqueda, 2003: A hindcast simulation of Arctic and Antarctic sea ice variability, 1955–2001. *Polar Res.,* **22,** 91–98.

Flato, G. M., and W. D. Hibler III, 1995: Ridging and strength in modeling the thickness distribution of Arctic sea ice. *J. Geophys. Res.,* **100,** 18 611–18 626.

Gille, S. T., 2002: Warming of the Southern Ocean since the 1950s. *Science,* **295,** 1275–1277.

Hibler, W. D., III, 1980: Modeling a variable thickness sea ice cover. *Mon. Wea. Rev.,* **108,** 1943–1973.

Jacka, T. H., and W. F. Budd, 1998: Detection of temperature and sea-ice-extent change in the Antarctic and Southern Ocean, 1949–96. *Ann. Glaciol.,* **27,** 637–640.

Jeffries, M. O., K. Morris, T. Maksym, N. Kozlenko, and T. Tin, 2001: Autumn sea ice thickness, ridging and heat flux variability in and adjacent to Terra Nova Bay, Ross Sea, Antarctica. *J. Geophys. Res.,* **106,** 4437–4448.

Kalnay, E., and Coauthors, 1996: The NCEP/NCAR 40-Year Reanalysis Project. *Bull. Amer. Meteor. Soc.,* **77,** 437–471.

Kwok, R., and J. C. Comiso, 2002: Spatial patterns of variability in Antarctic surface temperature: Connections to the Southern Hemisphere Annular Mode and the Southern Oscillation. *Geophys. Res. Lett.,* **29,** 1705, doi:10.1029/2002GL015415.

Levitus, S., J. L. Antonov, T. P. Boyer, and C. Stephens, 2000: Warming of the world ocean. *Science,* **287,** 2225–2229.

——, J. Antonov, and T. Boyer, 2005: Warming of the world ocean, 1955–2003. *Geophys. Res. Lett.,* **32,** L02604, doi:10.1029/2004GL021592.

Liu, J., J. A. Curry, and D. G. Martinson, 2004: Interpretation of recent Antarctic sea ice variability. *Geophys. Res. Lett.,* **31,** L02205, doi:10.1029/2003GL018732.

Martinson, D. G., P. D. Killworth, and A. L. Gordon, 1981: A convective model for the Weddell polynya. *J. Phys. Oceanogr.,* **11,** 466–488.

Maykut, G. A., 1986: The surface heat and mass balance. *The Geophysics of Sea Ice,* N. Untersteiner, Ed., Plenum, 489–549.

——, and M. G. McPhee, 1995: Solar heating of the Arctic mixed layer. *J. Geophys. Res.,* **100,** 24 691–24 704.

McPhee, M. G., C. Kottmeier, and J. H. Morison, 1999: Ocean heat flux in the Central Weddell Sea during winter. *J. Phys. Oceanogr.,* **29,** 1166–1179.

Parkinson, C. L., 2002: Trends in the length of the Southern Ocean sea-ice season, 1979–99. *Ann. Glaciol.,* **34,** 435–440.

Powell, D. C., T. Markus, and A. Stössel, 2005: Effects of snow depth forcing on Southern Ocean sea ice simulations. *J. Geophys. Res.,* **110,** C06001, doi:10.1029/2003JC002212.

Rayner, N. A., D. E. Parker, E. B. Horton, C. K. Folland, L. V. Alexander, D. P. Rowell, E. C. Kent, and A. Kaplan, 2003: Global analyses of sea surface temperature, sea ice, and night marine air temperature since the late nineteenth century. *J. Geophys. Res.,* **108,** 4407, doi:10.1029/2002JD002670.

Rothrock, D. A., Y. Yu, and G. A. Maykut, 1999: Thinning of the Arctic sea ice cover. *Geophys. Res. Lett.,* **26,** 3469–3472.

Santer, B. D., T. M. L. Wigley, J. S. Boyle, D. J. Gaffen, J. J. Hnilo, D. Nychka, D. E. Parker, and K. E. Taylor, 2000: Statistical significance of trends and trend differences in layer-average atmospheric temperature time series. *J. Geophys. Res.,* **105,** 7337–7356.

Smith, R. D., J. K. Dukowicz, and R. C. Malone, 1992: Parallel ocean general circulation modeling. *Physica D,* **60,** 38–61.

Thomas, R., and Coauthors, 2004: Accelerated sea-level rise from the west Antarctica. *Science,* **306,** 255–258.

Thompson, D. W. J., and J. M. Wallace, 2000: Annular modes in extratropical circulation. Part II: Trends. *J. Climate,* **13,** 1018–1036.

Wadhams, P., M. A. Lange, and S. F. Ackley, 1987: The ice thickness distribution across the Atlantic sector of the Antarctic Ocean in midwinter. *J. Geophys. Res.,* **92,** 14 535–14 552.

Wilks, D. S., 1995: *Statistical Methods in the Atmospheric Sciences*. Academic Press, 467 pp.

Yuan, X., and D. G. Martinson, 2000: Antarctic sea ice extent variability and its global connectivity. *J. Climate,* **13,** 1697–1717.

Zhang, J., 1993: A high resolution ice-ocean model with imbedded mixed layer. Ph.D. thesis, Dartmouth College, 229 pp. [Available from Dartmouth College, Hanover, NH 03755.]

——, and D. A. Rothrock, 2001: A thickness and enthalpy distribution sea-ice model. *J. Phys. Oceanogr.,* **31,** 2986–3001.

——, and ——, 2003: Modeling global sea ice with a thickness and enthalpy distribution model in generalized curvilinear coordinates. *Mon. Wea. Rev.,* **131,** 681–697.